Proceedings Paper:
Turnbull, R.P. orcid.org/0000-0001-7334-0880, Evans, E. and Dehghani-Sanij, A.A. (2023) Development and Validation of a Flexible Sensing Array for Placement within the Physical Human-Exoskeleton Interface. In: Proceedings of 2023 International Conference on Rehabilitation Robotics (ICORR). 2023 International Conference on Rehabilitation Robotics (ICORR), 24-28 Sep 2023, Singapore. IEEE . ISBN 979-8-3503-4275-8

https://doi.org/10.1109/ICORR58425.2023.10304686

Development and Validation of a Flexible Sensing Array for Placement within the Physical Human-Exoskeleton Interface

Rory Peter Turnbull[1], Elaine Evans[2] and Abbas Ali Dehghani-Sanij[1]

***Abstract*— Monitoring the human-exoskeleton interface (HEI) is vital for user safety in assistive exoskeletons. Considering interaction forces during design can improve comfort and efficiency and reduce resistance and inertia. Challenges include covering the lower limb area without interfering with user-robot interaction. This paper presents a force-sensitive resistor (FSR) based sensing sleeve for use within the HEI. The design includes 30 sensors and works independently of it to assess attachment modalities. System characterisation tests the system with human trials. Demonstrating that a low-cost, flexible sensing array can accurately monitor HEI. This provides a promising tool for assessing human-robot interaction and investigating wearable robotic device use.**

I. INTRODUCTION

Globally 15% of people experience disability, with 2-5% facing difficulty in daily life [1]. Exoskeletons have seen significant developments addressing medical, industrial and military sectors [2]. In 2018, the first medical exoskeleton achieved EU approval with a CE mark [3].

The investigation of human-exoskeleton interaction is currently lacking. Highlighted by Beckerle et al. [4] (2017) and more recently by Massardi et al. [5] (2022).

User comfort is a key factor in wearable robotics, as it affects device adoption, synergy with humans, and user safety. Greater loads can be tolerated with increasing stimulus [6]. When pressures exceed average capillary pressure (6.27 kPa) [7], blood vessel constriction reduces oxygen flow to the tissue. This can lead to pressure injuries and nerve damage, making users unable to detect discomfort. Thus, characterizing and monitoring interaction forces during exoskeleton use is crucial, especially for vulnerable users.

Various methods have been implemented to evaluate HEI, such as load cells [8], [9], inductive coils [10] and fibre-optics [11]. DC motors and fero-magnetic construction materials are common in exoskeletons. The related magnetic fields could significantly affect device accuracy. Additionally, the size constraints involved in HEI can limit implementation. The HEI involves two planes with three axes of motion: shear and normal, which involve sliding and perpendicular forces, respectively. Shear forces at the HEI are essential for user comfort and safety due to their link with tissue damage, but slim-form shear sensors capable of placement within the HEI are not commercially available.

[1]R.P. Turnbull and A.A.Dehghani-Sanij are with the School of Mechanical Engineering, University of Leeds, LS2 9JT, UK (Email R.P.Turnbull@Leeds.ac.uk,A.A.Dehghani-Sanij@Leeds.ac.uk)

[2]Elaine Evans is with the School of Design, University of Leeds. (Email: E.L.Evans@leeds.ac.uk)

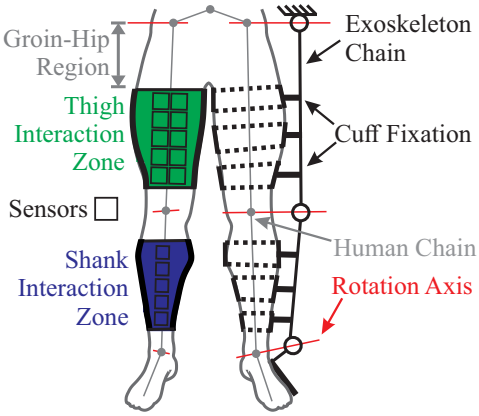

Fig. 1. Lower limb exoskeleton interaction. Right: Cuff attachment. Left: Green = thigh interaction zone and blue = shank interaction zone

FSRs embedded in attachment sites provide normal force data [12], [13]. These sensors have been implemented in arrays [13], [14] and embedded within attachment cuffs [15]. Recent advances enable the use of textile-based transducers. Quinlivan et al. [16] sandwiched piezo-resistive and conductive fabrics to produce a pressure mapping sheet with a 2cm resolution. Limb curvature could hinder the implementation of these sheets in attachment sites. Luo et al. [17] used piezo-resistive fibres to form a woven sensing skin. The proposed system aimed to use affordable, commercially available technology. Custom yarns and structures are impractical to replicate at this time but are promising for exploring HEI as technology develops in future years. Commercialised sensing systems exist, such as XSENSOR [Calgary, AB, Canada], Kitronyx [Seoul, Korea], Novel [Munich, Germany] and Tekscan [Norwood, MA, USA]. We propose a low-cost distributed system built from base components rather than full products, which may be limited by software and acquisition units.

We propose a low-cost, flexible sensing array to assess forces in HEI. We excluded shear sensing due to limited commercial availability. We discuss the system's design, characterise sensor performance and evaluate with three healthy participants.

II. DESIGN

Attachment cuffs are a common exoskeleton fixation method [2]. We propose a sensing sleeve worn during testing instead of integrating sensors in the exoskeleton cuffs (Fig. 1). Maintaining sensor position and array size across attachment modalities while covering the interaction zones (IZs;

Fig. 1) and excluding high-movement areas around joints. Internal material forces and structural components maintain sensor position.

A. Sensor Selection

FSRs were selected for their cost, maturity, speed of installation, ease of use, and size. To avoid affecting the HEI response, minimizing sensor size is key. FSRs operate through a piezoelectric active area with increased conductivity under pressure. Jones and Hooper [18] showed that layered materials do not affect readings ($P < 0.05$), allowing placement over clothes.

FSR-406 sensors [Interlink Electronics, CA, USA] were selected. It has been demonstrated that damage can occur after prolonged exposure to 6.27kPa (9.1N) [7]. Force values are calculated by applying the pressure over the FSR-406 active area (38.1×38.1 mm).

B. Sensor Housing

FSR sensors can be affected if loaded through their non-conductive perimeter. Sensor housing was developed to protect FSRs from the environment. Featuring an inner island layer (38.1×38.1 mm) to aid force distribution. Offset from the perimeter by an H-shaped top layer (green in Fig.2). Semi-spheres have been proposed for smaller form factor FSRs [13], [19]. The silicone rubber housing material was chosen based on Solis-Ortega et al. [20].

Wettenschwiler et al. [14] identified that skin-based force sensors were adversely affected by bony prominences, causing bending and humidity changes. Sensors are placed where there's soft tissue aside from the anterior shank. Bending causes inaccurate voltage readings in FSRs due to their piezoelectric structure. Unlike rigid designs, which remove bending by placing the FSR within a rigid structure [15], we designed a flexible system that could be worn as clothing. Sensors were reinforced with a 1.5mm aluminium plate, creating rigid regions within a flexible structure and allowing movement between sensors.

C. Materials

When body temperature rises, sweat is released to regulate it. Sensors around the limb increase local temperature and moisture, which can lead to slip, increasing the risk of skin irritation and surface damage. The humidity and potential for slip necessitated breathable materials; however, the electronics and housing are not breathable, so some moisture buildup is possible. Further testing must be done to characterize this.

A fabric blend of nylon (83%) and Lycra (17%) was chosen for comfort and flexibility [UK Fabrics Online]. The Lycra can stretch 2.4× before plastic deformation. Facilitating limb circumference changes attributed to muscular contraction. Nylon (100%) pockets (Fig. 2) were included for stability with sensor housings, laser-cut for precision. Material extension covered the 5th-95th percentile users [21]. Care was taken joining layers of nylon and Lycra to prevent internal stresses that could generate false signals from the sensors.

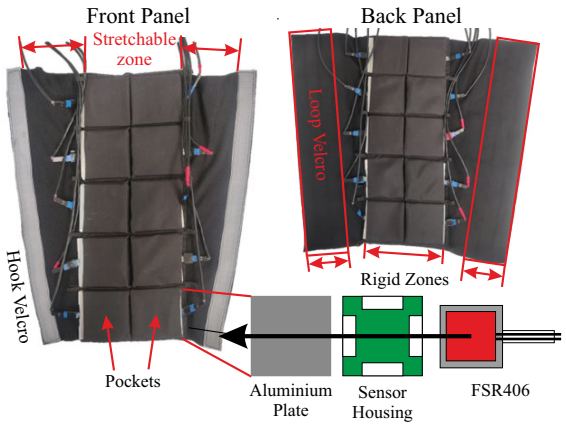

Fig. 2. Sensing sleeve design Left: front, Right: back.

The design maintained the sensor placement while accommodating all sizes with one cuff. It used a Velcro seam along the sides (Fig. 2) and additional material to adjust for varying users' limb sizes. Excess material wrapped around smaller limbs with minimal impact on results [18]. Sleeve panel height remained consistent at 330 mm and 380 mm for the thigh and shank, respectively. Width tapered distally, 205 mm to 140 mm for the shank (46%) and 300 mm to 210 mm (43%) and 380 mm to 290 mm (31%) for the thigh front and back. Lycra stretch and Velcro adjustment allowed a fit for 95% of the population with up to 46% extra extension.

Each sleeve was made of three panels. The central Nylon panel comprised two and one columns centred on the thigh and shank, respectively. Thigh columns were centred on a patella tendon to the groin axis. The shank column was centre aligned with the knee and ankle. Wires protruded to opposite sides. Lycra formed the outer panels. The Lycra was sewn between nylon layers to maintain joint integrity. The Lycra-nylon sleeve expansion ensures a consistent position among users. The horizontal position is sustained through internal Lycra forces, while the vertical position is maintained through loops of material and a belt. It is placed over clothing to protect the subject from shear forces. The sleeve houses 30 sensors in two 2×5 arrays and two 1×5 arrays for the thigh and shank (Fig. 2).

D. Data Acquisition

We used a MyRio running LabVIEW [National Instruments, TX, USA] with Multiplexers (MUXs) [CD74HC4067, Texas Instruments, TX, USA] to acquire FSR voltage output. LabVIEW provided I2C MUX/de-MUX control and synchronisation across FSR arrays, then formatted the data for Matlab processing[MathWorks, MA, USA]. MUXs minimised circuit complexity and extended sensor capacity.

The electronics were miniaturised to 40×50 mm circuit boards featuring multiplexers, voltage dividers (10 kΩ), and capacitors (0.1 μF) for signal stability. A MyRio interface board provided MUX control signal splitting and connectivity.

Human motion occurs at a maximum of 15 Hz [22], we selected a 100 Hz sampling frequency. MUXs split the

Fig. 3. Test subject in sensing sleeve and exoskeleton with covered sleeve areas highlighted

sensors into groups of five and ten, with the 16-channel MUX control running in parallel. Empty channels were grounded, and data was discarded. The system operated at 1.6 kHz, meeting the desired sensor frequency.

E. Sensor Characterisation

Tests were conducted to analyse FSR performance, including repeatability, hysteresis, bending and drift.

We assessed FSR406 cyclic loading repeatability using a single-column Instron 5943 and a 500N load cell [Instron 2580-500N, Wycombe, UK]. Six cycles of 0-60N at 0.03mm/s resulted in a percentage error of ±1.07-3.22% in four sensors (Fig. 4a), two sensors were outside the manufacturer's stated ±5% margin (±5.30, ±5.71%). The average inter-sensor repeatability was 23%.

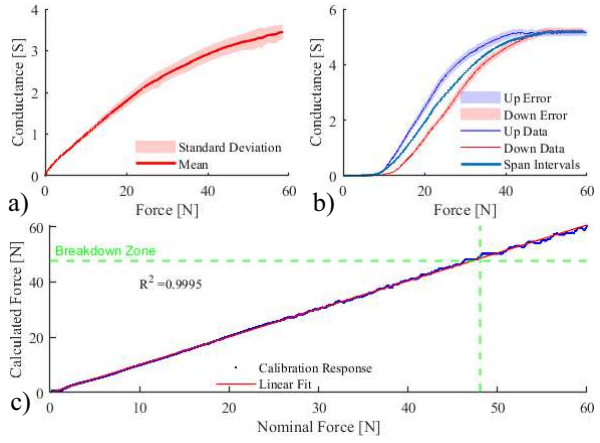

Fig. 4. FSR characterisation a) Cyclic loading, b) hysteresis and c) linearity.

We evaluated five sensors for hysteresis in a similar experimental setup, as per ISO 61298-2:2008 [23], with five repetitions. Sensors loaded from 0 to 60 Newtons at 0.0025 mm/s and returned with an average hysteresis error of 5.36% (Fig 4b), within the manufacturer's 10% limit.

To validate protection from external flexion, arcs were 3D printed in PLA [Raise 3D, CA, USA] based on limb circumference. The curvatures were calculated from the limb circumference data of each section [21]. Arc curvature was determined from the upper and lower thigh and shank, respectively: ThU 263mm, ThL 148mm, ShU 109mm and ShL 59mm.

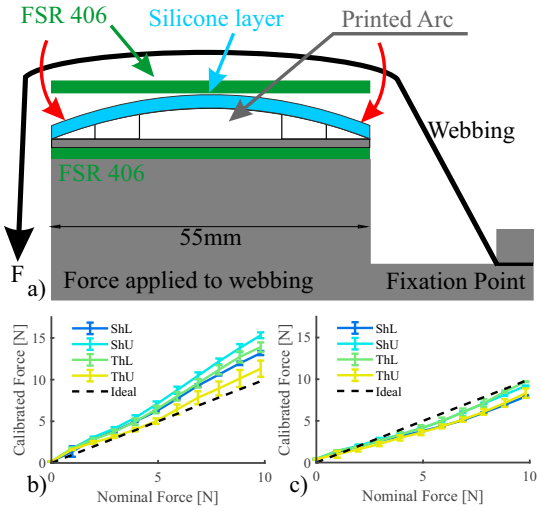

Fig. 5. FSR bend test set up and reinforcement results.

A skin simulant was made with Ecoflex 00-30 [Smooth-On Inc., PA, USA], with comparable mechanical properties to skin [24]. Sensors were loaded from 0-10 Newtons at intervals of 1 Newton, with 5 repeats and a 30-second relaxation period. Bending was found to result in up to 150% erroneous force (Fig. 6a). Further work is needed to determine the impact of continuous use.

Reinforcement with a 1.5 mm aluminium plate was found to account for the effect with an RMSE of 0.57-1.2 (Fig. 6b) compared to without (Fig. 6a), where RMSE reached 2.33-3.88. Although the addition of plates reducing system softness, the supporting structures maintain overall flexibility.

FSRs were tested with a static 3 N load for three repetitions, a third of capillary pressure [7]. The average drift was 0.16 N amounting to a 6.7% error, similar to the sensor repeatability. Since the application is dynamic, drift should have a minimal effect.

F. Calibration

Based on the FSR406 active area and a maximum capacity of 100 N, the FSRs were calibrated up to 60 N, three times greater than the range of interest (0-20 N), with force necessary to shut capillaries at 6.27 kPa (9.1 N).

With a sensor repeatability ±23%, the 30 sensors are individually calibrated. Sensors were uniformly loaded at 0.03mm/s 10 times between 0-60N/ Instron load data was collected and sensor output converted from voltage to conductance (Equation 1). A conductance-based approach benefits from a linear response in the 0-10N range and sensitive low force accuracy, which suited the 0-20N range of interest.

$$G = \frac{1}{MR \times \left(\frac{V_{in}}{V_{out}} - 1\right)} \tag{1}$$

Where G = conductance (S), MR = measuring resistor ($10k\Omega$), V_{in} = supply voltage (5v) and V_{out} = FSR output. We used curve fitting to produce a five-degree polynomial model of conductance vs applied force using MATLAB's curve fitting toolbox using a linear least square regression method.

$$F = P_1 \times G^5 + P_2 \times G^4 + P_3 \times G^3 + P_4 \times G^2 + P_5 \times G + P_6 \quad (2)$$

Where F = Force [N], G = Conductance [S], P_{1-6} = five degree polynomial parameters. The calibration model was validated by passing a sixth data set through it and quantifying linearity with correlation (R^2 values of 0.9931 ±0.0235 across 30 sensors. Demonstrating a significant relationship and model applicability. At higher forces, the calibration model is less stable (Fig. 4c). HEI forces usually occur in the 0-20N range, minimizing its impact. Schofield et al. [25] found that temperature had no significant effect on FSR 406 performance, though it did affect other FSRs.

III. Experimental Evaluation

We evaluated the system's performance on three healthy male subjects (age 28±1.4, height [m] = 1.8±0.1). University Ethics Board approval was obtained (MEEC 18-030).

The participants wore the sensing system and used audio/visual aids to ensure a stride length and cadence of 0.7 m/s, half the average walking pace. Markers were placed every 0.7 m over 5 m, with average stride length relative to participant height. Controlling for these variables helps assess system repeatability. Exoskeleton gait typically deviates from natural gait. Control measurements were taken with only the sensing system.

Participants donned a custom six DOF lower limb exoskeleton with a single rotational joint at the hip, knee and ankle. Three attachment cuffs per link - across the IZs - were selected for assessment. It is noted exoskeletons do not commonly include all three. We used three to fully assess the system. Each cuff was aligned with a row of sensors. The length and placement of each cuff were individualised to user limb segment dimensions. A placement model (Equation 3) was developed from the preliminary testing of four subjects.

$$(ThLen \times 87.7\%) \times \frac{n}{6} + (ThLen \times (1 - 87.7\%) \quad (3)$$

Where ThLen = thigh length and n = adjusted cuff numerator (1.3,3,4.8). The 87.7% accounts for the portion of femur length that cannot accommodate exoskeleton attachment (Fig. 1). Adjustments were made to the numerators to allow for joint movement, as shank cuffs were spaced at intervals of $\frac{n}{6}$ with n values of 1.4, 3.0 and 4.7, where the first value resided below the tibia tuberosity. The model was validated using three subjects Accuracy was 98%. Further testing is required to validate against a larger population.

Participants wore leggings to avoid wrinkles under the sensors. Participants stayed still, and the first eight seconds were averaged to get a base reading. This was used to detect changes from the sensor's start reading. Participants completed five repetitions of level gait, comprised of four gait cycles in a line, with and without the exoskeleton. The gait cycle force responses were compared, excluding the first and last cycles.

A 100th-order low-pass finite response impulse filter with a 5Hz cut-off was used to maintain signal waveform integrity. The Root Mean Square Error (nRMSE) was normalised against the response range indicating the system's error. Datasets of individual and average results were collected for intra-subject variability and inter-subject repeatability analysis.

IV. Results

A. Force Response

Peak, average and minima force values were collated from the two gait cycles used per repeat to summarise the data(Fig.6). All sensors achieved output values significantly greater than the control group with non-overlapping 95% confidence intervals. Participants' movement does not significantly impact performance during gait with a force response of 0.27 ±0.2 N observed. The anterior and posterior thigh panels exhibited an average force of 2.17 N ±1.79. Interaction force increased distally, peaking in sensors five and nine at 5.3 N ±0.3 N (Fig. 6 sensors 1-20). The posterior thigh array exhibited a 1.65 N smaller response compared to the anterior thigh. The shank saw larger force increases without an exoskeleton attached, double those of the thigh at 1.64 N ±0.75 and 1.44 N ±0.87 for the anterior and posterior (Fig. 6 sensors 21-30). The highest interaction force response observed was the posterior shank (7.80 ± 2.53 N) temporally moving above the 9.1N required to close capillaries.

B. Repeatability

The responses to five repetitions were compared for each participant (Fig. 7a). Intra-subject repeatability was assessed via the average response across the five pairs (Fig. 7b) and overall waveform (Fig. 7c). Peaks were aligned from the second/third gait cycle peaks, taking into account audio/visual queues for consistency. The system's intrasubject repeatability was evaluated via nRMSE; subjects one, two, and three achieved 20% ±12%, 20% ±15%, and 14% ±10%, respectively (example in Fig. 7a).

Inter-subject repeatability is seldom reported in system design, so we studied system intersubject variability. Isolated to a single gait cycle in Fig. 7b and three gait cycles in Fig. 7c. The analysis revealed greater variation between subjects, despite similar peak and trough values. The nRMSE was 35% ±28% higher than the average of all subjects.

V. Discussion

A. Force Response

We hypothesised that relaxed and contracted muscle states would influence HEI and FSR response. To account for subtle contraction-caused changes, we implemented a flexible system rather than a rigid cuff. Demonstrating the system's ability to account for subtle circumference changes in the control's low force response (0.27 ±0.2 N).

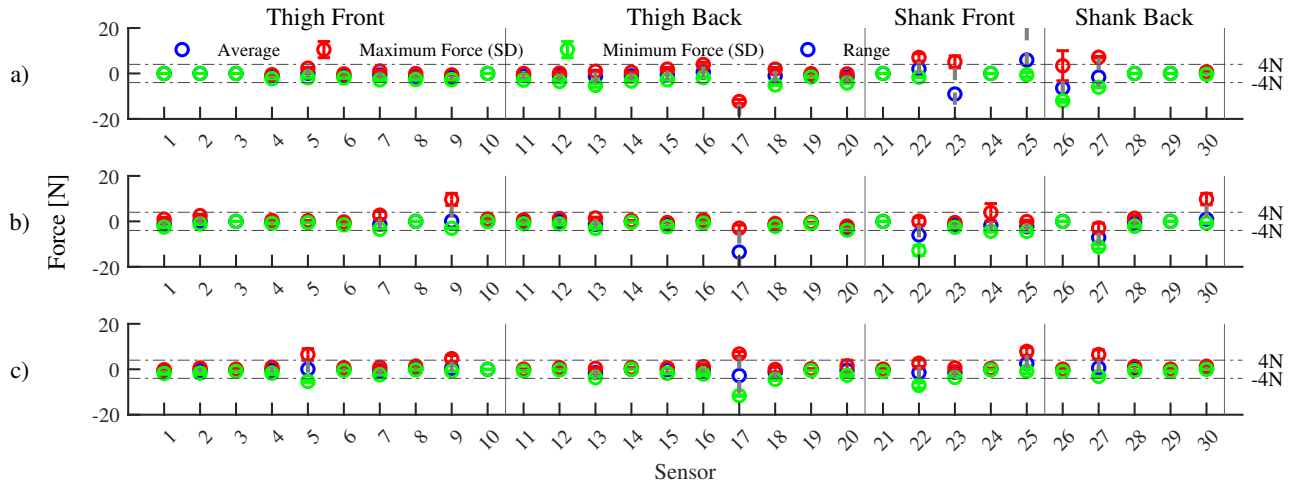

Fig. 6. Force response, thigh sensors 1-20 and shank 21-30 a) Subject 1, b) Subject 2 and c) Subject 3.

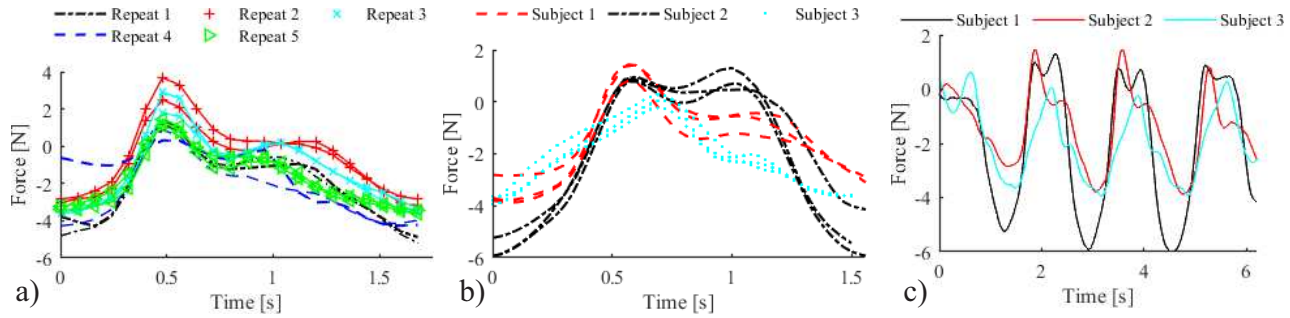

Fig. 7. Gait cycle force response repeatability, a) Subject 1 intrasubject (five repetitions), b) Intersubject, single cycle, c) Mean subject data.

Subjects 1-3 experienced force responses of ±4N, ±3N and ±2N, respectively (Fig. 6a-c). Exceptions occurred at sensors 23 and 25 on the shank, where forces of -20N and 23.9N were seen. This reduction in output could be due to calf contraction or cuff slip.

Forces increased distally in both thigh and shank, with the highest of 7.8 N ±2.53 N, near the 9.1 N compression limit. Most sensors (75%) registered force in the ±4N range. Sensors near the attachment cuff experienced higher forces. The highest forces in the posterior shank peaked at 17 N, but only briefly. The posterior thigh experienced 1.68 N lower forces than the anterior, on average. The passive exoskeletons likely cause this effect as the user's forward motion pushes against the cuff. Further testing will confirm if this is reversed in an active system. Shank muscle distribution often decreases distally, but force response increases. This indicates that the increase is due to a combination of more rigid structures in the anterior tibia and reduced elastic material. The knee has more motion range than the foot-exoskeleton anchor point, creating greater resistance when it moves at the shank attachment.

Studies have evaluated exoskeleton performance and new sensing technology interactions. Li et al. [9] implemented load cells [ATI Mini45-SI-145-5] between the attachment cuff and exoskeleton, observing interaction forces of ±5 N to ±10 N. Work by Rathore et al. [12] implemented FSR sensors at the pHRI and achieved responses up to 8 N during level gait, similar to the results of this study. Two studies showed higher interaction forces of 10-30 N during gait using light-based assessment [11]. With exoskeleton development and added joint torque, the force response could significantly increase.

B. Repeatability

In wearable robotic interaction studies, intra-subject error reporting is common. Georgarakis et al. [8] proposed a system for assessing HEI with a force sensor, with up to 28.7% error. Wettenschwiler et al. [14] recorded an error of 31% . Hsiao et al. [26] reported an error of 34% in a shoe-based system. Achieving error similar to this study.

The inter-subject error of 35% ±28% was expected due to the difficulty of HEI and soft tissue. The intra-subject error remained consistent at 18% ±3%. Controlling for several variables, errors likely stem from user differences, given the intra-subject repeatability. A high inter-subject error implies the need for individual data assessment. nRMSE error, calculated from an average waveform of all subjects, was more significant. More testing is required to fully characterize repeatability, including larger test populations and repeated donning and doffing. The proposed system will be pursued further to evaluate its performance in assessing HEI. Overall, the results are promising compared to similar systems.

C. Limitations

Though three participants were included, further testing is needed to measure efficacy for the general population. The current system lacks shear assessment. With technological advancement, we will strive for the integration of shear measurement while keeping the format slim and body-conforming. This system lacks sensors on the medial and lateral sides of the limbs. Forward motion interacts at the rear and front, but ill-fitting exoskeletons and unexpected motions can affect the lateral regions. Future development should focus on covering these areas. The implementation of shear sensing lends itself to gaining key insights. Calibration utilised even force distribution on the housing surface. Further testing should be done to assess calibration performance and load distribution with sub-area loads. The system was assessed under controlled gait settings. Future work will assess user performance in natural gait to evaluate exoskeleton performance. Further assessment is needed to evaluate the errors caused by frequent wearing of the system, such as donning and doffing.

VI. Conclusion

In our work, we have provided a proof of concept for using a flexible sensing array to assess HEI as an assistive exoskeleton development aid. Our results show that our sensing array effectively assesses HEI forces with greater repeatability than other systems while reporting force values similar to the literature. A key advantage is the ease with which it can be positioned and its ability to be used with a range of systems. Approaches such as this are key to widening the knowledge in HEI. The proposed system is a promising tool for informing assistive exoskeleton design.

References

[1] J. Bickenbach, "The world report on disability," Tech. Rep. 5, World Health Organisation, aug 2011.

[2] A. Rodríguez-Fernández, J. Lobo-Prat, and J. M. Font-Llagunes, "Systematic review on wearable lower-limb exoskeletons for gait training in neuromuscular impairments," *Journal of NeuroEngineering and Rehabilitation*, vol. 18, no. 1, p. 22, 2021.

[3] D. Kirsh, "Gogoa Mobility Robots wins CE Mark for Hank exoskeleton," 2018.

[4] P. Beckerle, G. Salvietti, R. Unal, D. Prattichizzo, S. Rossi, C. Castellini, S. Hirche, S. Endo, H. Ben Amor, M. Ciocarlie, F. Mastrogiovanni, B. D. Argall, and M. Bianchi, "A Human-Robot Interaction Perspective on Assistive and Rehabilitation Robotics," *Frontiers in Neurorobotics*, vol. 11, 2017.

[5] S. Massardi, D. Rodriguez-Cianca, D. Pinto-Fernandez, J. C. Moreno, M. Lancini, and D. Torricelli, "Characterization and Evaluation of Human–Exoskeleton Interaction Dynamics: A Review," *Sensors*, vol. 22, p. 3993, may 2022.

[6] T. Kermavnar, K. J. O'Sullivan, V. Casey, A. de Eyto, and L. W. O'Sullivan, "Circumferential tissue compression at the lower limb during walking, and its effect on discomfort, pain and tissue oxygenation: Application to soft exoskeleton design," *Applied Ergonomics*, vol. 86, no. June 2019, 2020.

[7] L. Agam and A. Gefen, "Pressure ulcers and deep tissue injury in wheelchair users: A bioengineering perspective," *International Journal of Therapy and Rehabilitation*, vol. 15, no. 2, pp. 90–99, 2008.

[8] A. M. Georgarakis, R. Stampfli, P. Wolf, R. Riener, and J. E. Duartc, "A Method for Quantifying Interaction Forces in Wearable Robots," *Proceedings of the IEEE RAS and EMBS International Conference on Biomedical Robotics and Biomechatronics*, vol. 2018-Augus, pp. 789–794, 2018.

[9] J. Li, S. Zuo, C. Xu, L. Zhang, M. Dong, C. Tao, and R. Ji, "Influence of a Compatible Design on Physical Human-Robot Interaction Force: a Case Study of a Self-Adapting Lower-Limb Exoskeleton Mechanism," *Journal of Intelligent and Robotic Systems*, 2019.

[10] H. Wang, D. Jones, G. de Boer, J. Kow, L. Beccai, A. Alazmani, and P. Culmer, "Design and Characterization of Tri-Axis Soft Inductive Tactile Sensors," *IEEE Sensors Journal*, vol. 18, pp. 7793–7801, oct 2018.

[11] A. G. Leal-Junior, C. R. Díaz, M. J. Pontes, C. Marques, and A. Frizera, "Polymer optical fiber-embedded, 3D-printed instrumented support for microclimate and human-robot interaction forces assessment," *Optics and Laser Technology*, vol. 112, no. October 2018, pp. 323–331, 2019.

[12] A. Rathore, M. Wilcox, D. Z. M. Ramirez, R. Loureiro, and T. Carlson, "Quantifying The Human-Robot Interaction Forces Between A Lower Limb Exoskeleton And Healthy Users," 2016.

[13] J. Bessler, L. Schaake, R. Kelder, J. H. Buurke, and G. B. Prange-Lasonder, "Prototype Measuring Device for Assessing Interaction Forces between Human Limbs and Rehabilitation Robots - A Proof of Concept Study," in *2019 IEEE 16th International Conference on Rehabilitation Robotics (ICORR)*, pp. 1109–1114, June 2019. ISSN: 1945-7901.

[14] P. D. Wettenschwiler, R. Stämpfli, S. Lorenzetti, S. J. Ferguson, R. M. Rossi, and S. Annaheim, "How reliable are pressure measurements with Tekscan sensors on the body surface of human subjects wearing load carriage systems?," *International Journal of Industrial Ergonomics*, vol. 49, no. March 2019, pp. 60–67, 2015.

[15] K. Ghonasgi, S. N. Yousaf, P. Esmatloo, and A. D. Deshpande, "A Modular Design for Distributed Measurement of Human–Robot Interaction Forces in Wearable Devices," 2021.

[16] B. Quinlivan, A. T. Asbeck, D. Wagner, T. Ranzani, S. Russo, and C. J. Walsh, "Force Transfer Characterization of a Soft Exosuit for Gait Assistance," *Volume 5A: 39th Mechanisms and Robotics Conference*, pp. 1327–1334, 2015.

[17] Y. Luo, Y. Li, P. Sharma, W. Shou, K. Wu, M. Foshey, B. Li, T. Palacios, A. Torralba, and W. Matusik, "Learning human–environment interactions using conformal tactile textiles," *Nature Electronics*, vol. 4, pp. 193–201, Mar. 2021. Number: 3 Publisher: Nature Publishing Group.

[18] G. R. Jones and R. H. Hooper, "The effect of single- or multiple-layered garments on interface pressure measured at the backpack-shoulder interface," *Applied Ergonomics*, vol. 36, no. 1, pp. 79–83, 2005.

[19] C. Castellini and V. Ravindra, "A wearable low-cost device based upon Force-Sensing Resistors to detect single-finger forces," in *IEEE/RAS-EMBS International Conference on Biomedical Robotics and Biomechatronics (BioRob)*, Aug. 2014.

[20] R. D. Solis-Ortega, A. A. Dehghani-Sanij, and U. Martinez-Hernandez, "The Assessment of Viscoelastic Models for Nonlinear Soft Materials," *Proceedings of the IEEE RAS and EMBS International Conference on Biomedical Robotics and Biomechatronics*, vol. 2018-Augus, pp. 1274–1279, 2018.

[21] C. C. Gordon, T. Churchill, C. E. Clauser, J. T. Mcconville, I. O. Tebbetts, and R. a. Walker, "2012 Anthropometric Survey of U . S . Army Personnel : Methods and Summary Statistics," Tech. Rep. April 2012, U.S. Army Natick Soldier Research, Natick, 2012.

[22] H. J. Freund, "Time control of hand movements," *Progress in Brain Research*, vol. 64, no. C, pp. 287–294, 1986.

[23] BSI, "BSI Standards Publication Process measurement and control devices — General methods and procedures for evaluating performance — Part 3 : Tests for the effects of influence quantities," 2008.

[24] K. Ogata and T. Yamamoto, "A fundamental study of light and flexible wearable robot assisting to recover movement functions," in *The 23rd IEEE International Symposium on Robot and Human Interactive Communication*, pp. 90–95, 2014.

[25] J. S. Schofield, K. R. Evans, J. S. Hebert, P. D. Marasco, and J. P. Carey, "The effect of biomechanical variables on force sensitive resistor error: Implications for calibration and improved accuracy," *Journal of Biomechanics*, vol. 49, no. 5, pp. 786–792, 2016.

[26] H. Hsiao, J. Guan, and M. Weatherly, "Accuracy and precision of two in-shoe pressure measurement systems," *Ergonomics*, vol. 45, pp. 537–555, jun 2002.